

Photonic temporal-mode multiplexing by quantum frequency conversion in a dichroic-finesse cavity

DILEEP V. REDDY^{1,*} AND MICHAEL G. RAYMER¹

¹*Oregon Center for Optical, Molecular, and Quantum Science, and Department of Physics, 1274 University of Oregon, Eugene, OR 97403, USA*

*dileep@uoregon.edu

Abstract: Photonic temporal modes (TMs) form a field-orthogonal, continuous-variable degree of freedom that is in principle infinite dimensional, and create a promising resource for quantum information science and technology. The ideal quantum pulse gate (QPG) is a device that multiplexes and demultiplexes temporally orthogonal optical pulses that have the same carrier frequency, spatial mode, and polarization. The QPG is the chief enabling technology for usage of orthogonal temporal modes as a basis for high-dimensional quantum information storage and processing. The greatest hurdle for QPG implementation using nonlinear-optical, parametric processes with time-varying pump or control fields is the limitation on achievable temporal mode selectivity, defined as perfect TM discrimination combined with unity efficiency. We propose the use of pulsed nonlinear frequency conversion in an optical cavity having greatly different finesse for different frequencies to implement a nearly perfectly TM-selective QPG in a low-loss integrated-optics platform.

References and links

1. M. G. Raymer and K. Srinivasan, “Manipulating the color and shape of single photons,” *Physics Today* **65**, 32 (2012).
2. P. C. Humphreys, W. S. Kolthammer, J. Nunn, M. Barbieri, A. Datta, and I. A. Walmsley, “Continuous-Variable Quantum Computing in Optical Time-Frequency Modes Using Quantum Memories,” *Physical Review Letters* **113**, 130502 (2014).
3. J. Nunn, L. J. Wright, C. Söller, L. Zhang, I. A. Walmsley, and B. J. Smith, “Large-alphabet time-frequency entangled quantum key distribution by means of time-to-frequency conversion,” *Opt. Express* **21**, 15959–15973 (2013).
4. L. J. Wright, M. Karpiński, C. Söller, and B. J. Smith, “Spectral shearing of quantum light pulses by electro-optic phase modulation,” *Phys. Rev. Lett.* **118**, 023601 (2017).
5. A. O. C. Davis, P. M. Saulnier, M. Karpiński, and B. J. Smith, “Pulsed single-photon spectrometer by frequency-to-time mapping using chirped fiber bragg gratings,” *Opt. Express* **25**, 12804–12811 (2017).
6. B. J. Smith and M. G. Raymer, “Photon wave functions, wave-packet quantization of light, and coherence theory,” *New Journal of Physics* **9**, 414 (2007).
7. B. Brecht, D. V. Reddy, C. Silberhorn, and M. G. Raymer, “Photon temporal modes: A complete framework for quantum information science,” *Phys. Rev. X* **5**, 041017 (2015).
8. A. Eckstein, B. Brecht, and C. Silberhorn, “A quantum pulse gate based on spectrally engineered sum frequency generation,” *Optics Express* **19**, 13370 (2011).
9. B. Brecht, A. Eckstein, A. Christ, H. Suche, and C. Silberhorn, “From quantum pulse gate to quantum pulse shaper—engineered frequency conversion in nonlinear optical waveguides,” *New Journal of Physics* **13**, 065029 (2011).
10. D. V. Reddy, M. G. Raymer, C. J. McKinstrie, L. Mejling, and K. Rottwitz, “Temporal mode selectivity by frequency conversion in second-order nonlinear optical waveguides,” *Optics Express* **21**, 13840–13863 (2013).
11. V. Ansari, M. Allgaier, L. Sasoni, B. Brecht, J. Roslund, N. Treps, G. Harder, and C. Silberhorn, “Temporal-mode tomography of single photons,” arXiv:1607.03001v1 (2016).
12. P. Manurkar, N. Jain, M. Silver, Y.-P. Huang, C. Langrock, M. M. Fejer, P. Kumar, and G. S. Kanter, “Multidimensional mode-separable frequency conversion for high-speed quantum communication,” *Optica* **3**, 1300–1307 (2016).
13. D. V. Reddy and M. G. Raymer, “Engineering temporal-mode-selective frequency conversion in nonlinear optical waveguides: from theory to experiment,” *Opt. Express* **25**, 12952–12966 (2017).
14. D. V. Reddy, M. G. Raymer, and C. J. McKinstrie, “Efficient sorting of quantum-optical wave packets by temporal-mode interferometry,” *Optics Letters* **39**, 2924–2927 (2014).
15. D. V. Reddy, M. G. Raymer, and C. J. McKinstrie, “Sorting photon wave packets using temporal-mode interferometry based on multiple-stage quantum frequency conversion,” *Phys. Rev. A* **91**, 012323 (2015).
16. T. Kobayashi, D. Yamazaki, K. Matsuki, R. Ikuta, S. Miki, T. Yamashita, H. Terai, T. Yamamoto, M. Kaoshi, and N. Imoto, “Mach-Zehnder interferometer using frequency-domain beamsplitter,” arXiv:1703.08114 (2017).

17. S. Ramelow, A. Farsi, S. Clemmen, D. Orquiza, K. Luke, M. Lipson, and A. L. Gaeta, "Silicon-nitride platform for narrowband entangled photon generation," arXiv:1508.04358 (2015).
18. N. Quesada and J. E. Sipe, "High efficiency in mode-selective frequency conversion," *Opt. Lett.* **41**, 364–367 (2016).
19. Z. Zheng and A. Weiner, "Coherent control of second harmonic generation using spectrally phase coded femtosecond waveforms," *Chemical Physics* **267**, 161 – 171 (2001).
20. Z. Zheng, A. M. Weiner, K. R. Parameswaran, M.-H. Chou, and M. M. Fejer, "Femtosecond second-harmonic generation in periodically poled lithium niobate waveguides with simultaneous strong pump depletion and group-velocity walk-off," *J. Opt. Soc. Am. B* **19**, 839–848 (2002).
21. J. I. Cirac, L. M. Duan, and P. Zöller, "Quantum optical implementation of quantum information processing," arXiv:quant-ph/0405030 (2004).
22. X.-H. Bao, A. Reingruber, P. Dietrich, J. Rui, A. Duck, T. Strassel, L. Li, N.-L. Liu, B. Zhao, and J.-W. Pan, "Efficient and long-lived quantum memory with cold atoms inside a ring cavity," *Nat. Phys.* **8**, 517–521 (2012).
23. J. Nunn, S. Thomas, J. H. D. Munns, K. T. Kaczmarek, C. Qiu, A. Feizpour, E. Poem, B. Brecht, D. J. Saunders, P. M. Ledingham, D. V. Reddy, M. G. Raymer, and I. A. Walmsley, "Theory of noise suppression in λ -type quantum memories by means of a cavity," arXiv:1601.00157v1 (2016).
24. D. V. Strelakov, A. S. Kowligy, Y.-P. Huang, and P. Kumar, "Optical sum-frequency generation in a whispering-gallery-mode resonator," *New Journal of Physics* **16**, 053025 (2014).
25. Q. Li, M. Davanco, and K. Srinivasan, "Efficient and low noise single-photon-level frequency conversion interfaces using Si_3N_4 microrings," in "2016 Progress in Electromagnetic Research Symposium (PIERS)," (2016), pp. 2574–2574.
26. X. Guo, C.-L. Zou, H. Jung, and H. X. Tang, "On-chip strong coupling and efficient frequency conversion between telecom and visible optical modes," *Phys. Rev. Lett.* **117**, 123902 (2016).
27. D. V. Strelakov, C. Marquardt, A. B. Matsko, H. G. L. Schwefel, and G. Leuchs, "Nonlinear and quantum optics with whispering gallery resonators," *Journal of Optics* **18**, 123002 (2016).
28. D. Burnham and R. Chiao, "Coherent Resonance Fluorescence Excited by Short Light Pulses," *Physical Review* **188**, 667–675 (1969).
29. M. J. Collett and C. W. Gardiner, "Squeezing of intracavity and traveling-wave light fields produced in parametric amplification," *Phys. Rev. A* **30**, 1386–1391 (1984).
30. M. G. Raymer and C. J. McKinstrie, "Quantum input-output theory for optical cavities with arbitrary coupling strength: Application to two-photon wave-packet shaping," *Phys. Rev. A* **88**, 043819 (2013).
31. Y.-Z. Sun, Y.-P. Huang, and P. Kumar, "Photonic nonlinearities via quantum zeno blockade," *Phys. Rev. Lett.* **110**, 223901 (2013).
32. J.-T. Shen and S. Fan, "Theory of single-photon transport in a single-mode waveguide. ii. coupling to a whispering-gallery resonator containing a two-level atom," *Phys. Rev. A* **79**, 023838 (2009).
33. I. M. Mirza, S. J. van Enk, and H. J. Kimble, "Single-photon time-dependent spectra in coupled cavity arrays," *J. Opt. Soc. Am. B* **30**, 2640–2649 (2013).
34. K. L. Tsakmakidis, L. Shen, S. A. Schulz, X. Zheng, J. Upham, X. Deng, H. Altug, A. F. Vakakis, and R. W. Boyd, "Breaking Lorentz reciprocity to overcome the time-bandwidth limit in physics and engineering," *Science* **356**, 1260–1264 (2017).

An important goal in quantum information science and technology is complete control of photonic states [1]. Beyond the polarization and transverse spatial degrees of freedom, the time-frequency degree of freedom is largely an untapped quantum resource [2–5]. Orthogonal temporal modes (TMs) are defined by the complex longitudinal wave-packet shape functions of pulsed modes of light [6]. They form a field-orthogonal, continuous-variable degree of freedom that is in principle infinite dimensional, and create a promising resource for quantum information science [7]. To fully exploit their use in a quantum network requires the ability to unitarily demultiplex arbitrary TM components from a light beam with near-unity efficiency and mode discrimination (i.e., no crosstalk). A device capable of such operations is known as a quantum pulse gate (QPG) [8, 9]. The ideal QPG must satisfy two conditions: (a) It must fully separate the desired TM component from the others without loss of photons, and (b) it must avoid contamination from orthogonal TM components in the "wrong" TM channels. When both of these are met, the QPG is said to have unit selectivity [10].

There exists a fundamental limit to selectivity of QPGs based on traveling-wave interactions in media with simple dispersion profiles, which enforces a trade-off between the two aforementioned conditions [10–13]. The best performing QPG proposed to date is based on temporal-mode interferometry (TMI) that performs pulsed, cascaded frequency conversion with multiple passes through standard dispersive nonlinear optical media (three-wave mixing in crystals or four-wave

mixing in fiber) [14–16]. The technique is a close relative of Ramsey interference of photons in a frequency-converting interferometer [15, 17]. In TMI, TMs from all participating carrier-frequency bands coherently reinteract at every stage, resulting in a selectivity enhancement that overcomes the single-stage maximum [18]. The gain in selectivity is very significant for even two-stage schemes, and is predicted to improve asymptotically with the number of stages [15]. While TMI has been shown to operate as predicted, it presents practical difficulties due to coupling losses and engineering/manufacturing constraints for integration.

A QPG that can multiplex and demultiplex field-orthogonal optical pulses is closely related to devices studied for coherent optical code multiple access (OCDMA) employing second-harmonic generation of phase-structured ultrafast pulses [19, 20]. Like the other implementations of coherent demultiplexers mentioned above, the TM selectivity of this scheme is limited by traveling-wave phenomena during nonlinear frequency conversion [20]. In a different research arena, optical-cavity-enhanced atomic-ensemble or solid-state quantum memories are known theoretically to have TM-selective qualities for coherent optical storage [21–23]. Finally, great technical advances have been made in design and fabrication of nonlinear-optical micro-ring resonators, and these have been employed for frequency conversion between telecom and visible bands via sum-frequency generation [24–27].

By combining insights from all the diverse areas discussed above, we have arrived at a means of using an optical micro-cavity with a large difference in finesse for two frequency bands participating in nonlinear frequency conversion by sum-frequency generation (SFG), to mimic the TM-selective behavior predicted for cavity-based atomic quantum memories. This all-optical “dichroic-finesse cavity” scheme provides a simple, realistic way to create a near-ideal add/drop (multiplexer/demultiplexer) device in a low-loss integrated-optics platform for use in quantum optical networks. By passing the control and signal pulses through the same frequency-converting medium many times, the device effectively performs TMI with a near-infinite number of stages, which explains its high TM selectivity. The proposed system operates without the need for atomic vapors or doped crystals. The weak signal pulse may be in a single-photon state (or any low-number Fock state), or in any other quantum state, such as squeezed vacuum. It can be temporally reshaped during the read-in and read-out process. The proposed scheme, while challenging to construct, relies only on already proven technology.

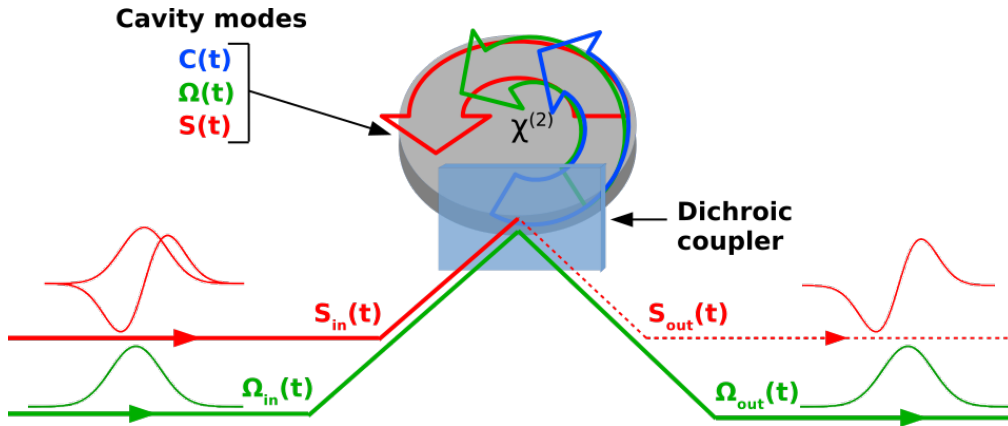


Fig. 1. Schematic of dichroic-finesse cavity filled with second-order nonlinear optical material. The converted field $C(t)$ is not shown exiting the cavity, as this occurs on much longer time scales.

Figure 1 shows a schematic diagram of the proposed micro-ring cavity system. $S(t)$ and $C(t)$ are the resonant cavity mode amplitudes of the two frequency bands that will interact via the

optical nonlinearity of the medium, which uniformly fills the cavity. The intracavity control field $\Omega(t)$ can be a single strong, coherent laser pulse if the process is utilizing three-wave mixing, or a combination (product) of two pulses if four-wave mixing is used. For definiteness, we will consider sum-frequency generation by three-wave mixing, but all results apply to four-wave mixing as well. For sum-frequency generation the frequencies are related by $\omega_s + \omega_\Omega = \omega_c$. For convenience we refer to ω_s as “red” and ω_c as “blue.”

The theoretical model presented below predicts that for a given temporal shape of the control field $\Omega(t)$ inside the cavity, only a single temporal mode of the incoming (red) signal field, called the target mode, will be frequency up-converted, creating narrowband (blue) light that is trapped in the cavity in the $C(t)$ mode. All TMs temporally orthogonal to the target mode will be transmitted into the $S_{\text{out}}(t)$ beam with the original (red) carrier frequency. The trapped blue light can subsequently be left to leak slowly from the cavity at later times, or it can be rapidly read out (ejected) from the cavity by applying a subsequent control pulse, which converts it back to red.

The temporal widths of the control field and the signal input $S_{\text{in}}(t)$ must be much longer than the cavity round-trip time, but much shorter than the cavity lifetime for the $C(t)$ mode. This leads to negligible leakage of the converted $C(t)$ amplitude from the cavity during the process. The $C(t)$ mode then becomes analogous to a coherent spin wave (for example) in a cold atomic ensemble. The cavity-coupling coefficients are assumed to put $S(t)$ in the “bad-cavity” limit. This finesse differential across the frequency bands is the key feature necessary to break the interaction symmetry and yield efficient TM multiplexing.

The solutions to the coupled-mode equations of motion can be expressed as linear integral scattering relations between input and output temporal modes using Green’s functions, which are functions of both an input-mode time argument and an output-mode time argument. For the process to be mode discriminatory, the Green’s functions should be separable in their time arguments, which is impossible for time-stationary processes. A key requirement for achieving Green’s function separability in previous (cavityless) approaches has been a large difference in the group velocities between the various frequency bands [10, 13–15]. This is required because orthogonal TMs can share very similar (even identical) temporal features in local time slices. For the QPG to perform different transformations on these two TMs, the full global mode structure needs to be surveyed by the device, as the effect (depletion/enhancement/phase-shift) on any given time slice should depend on features in all other time slices. Differing group velocities cause pulsed modes field amplitudes from different time slices to convect through each other, providing an effective means of carrying local mode information across different time slices. TMI operates by causing convecting pulses to overlap in spacetime over multiple stages, with the interaction being semi-perturbative during each stage. This avoids coherent-propagation ringing effects [28] induced by cascaded second-order nonlinearity [10, 19, 20], and ensures Green’s function separability even at high conversion efficiencies [18].

Our proposed scheme ensures inter-pulse convection by confining the TMs of one of the bands in physical space as the other TMs pass through it. Our design using a large difference in finesse across the frequency bands works for controls and signals with arbitrary relative group velocities, which is another advantage over (cavityless) traveling-wave QPG implementations.

We analyze the case of a nonlinear waveguide forming a resonant ring cavity, assuming frequencies that are phase matched for the control field $\Omega(t)$, signal $S_{\text{in}}(t)$, and converted $C(t)$. The key to is to have the cavity input-output coupling be frequency dependent, while still requiring that both modes have high finesse. With a very long, smooth input signal pulse, this allows the bad-cavity limit (only) for the S -field, meaning it tends to leak from the cavity relatively rapidly. Concurrently, we assume the cavity has much higher finesse for the C -field than for the S field. Then, we can frequency convert the short, “red” input pulse $S_{\text{in}}(t)$ into a long-lived, resonant cavity mode at the “blue” frequency ω_c trapped within the cavity before it slowly leaks exponentially from the cavity.

Within the adopted parameter ranges, the system is well described using the standard input-output theory of Collett and Gardiner [29]. The approximations leading to this formalism require very weak coupling of the cavity modes to external freely propagating modes, and spectral widths of all signals significantly narrower than the free-spectral range of the cavity [30].

The weak quantum signal fields within the cavity are represented by annihilation operators $S(t)$ for the “red” input field and $C(t)$ for the “blue” converted field, and satisfy commutators $[C(t), C^\dagger(t)] = 1$, $[S(t), S^\dagger(t)] = 1$. The input fields immediately outside of the coupling mirror are $S_{\text{in}}(t)$, $C_{\text{in}}(t)$, which satisfy $[A_j(t), A_k^\dagger(t')] = \delta_{jk} \delta(t-t')$, and the outgoing fields are $S_{\text{out}}(t)$, $C_{\text{out}}(t)$.

We take $\Omega(t)$ to be the intracavity control field in an auxiliary mode, which in the “bad-cavity” limit is simply proportional to an incident field $\Omega_{\text{in}}(t)$. We absorb the square-root of the control field energy into a nonlinear interaction parameter α such that $\Omega(t)$ is square-normalized to one. We assume both signal fields are exactly resonant with their cavity modes and there is no phase mismatch for the SFG process. Then the equations of motion within the cavity are [25, 31]:

$$\partial_t S(t) = i\alpha\Omega^*(t)C(t) - \tilde{\gamma}_s S(t) + \sqrt{2\gamma_s} S_{\text{in}}(t), \quad (1)$$

$$\partial_t C(t) = i\alpha\Omega(t)S(t) - \tilde{\gamma}_c C(t) + \sqrt{2\gamma_c} C_{\text{in}}(t). \quad (2)$$

where $\tilde{\gamma}_s = \gamma_s + \kappa_s$, $\tilde{\gamma}_c = \gamma_c + \kappa_c$. The (real) damping rates γ_j , κ_j ($j = s, c$) correspond to unitary decay from the cavity mode to the external modes, and nonunitary decay to internal dissipative loss, respectively. For simplicity, as in [23], we omit the Langevin noise operators associated with the dissipative loss, as they do not contribute to measured signal intensities. The input-output relations are (with a chosen phase convention):

$$S_{\text{out}}(t) = -S_{\text{in}}(t) + \sqrt{2\gamma_s} S(t), \quad C_{\text{out}}(t) = -C_{\text{in}}(t) + \sqrt{2\gamma_c} C(t). \quad (3)$$

In the following, we assume there is no external input to the C mode, so $C_{\text{in}}(t)$ is omitted.

Equations 2 and 3 are linear in field operators (although nonlinear with respect to the control field, here an undepleted coherent state). Therefore they can describe the Heisenberg-picture operator dynamics of any quantum state of light. In the case that only a single signal photon is present throughout the system, the variables can be interpreted as Schrodinger-picture state amplitudes [32, 33].

The first crucial assumption is that the cavity out-coupling rate γ_s for the input channel is large compared to the rate at which all the fields vary - set by $\tilde{\gamma}_s$, $\tilde{\gamma}_c$ and α , so we can apply the “bad-cavity” limit to $S(t)$. By setting $\partial_t S(t) \rightarrow 0$, we get

$$S(t) = i(\alpha/\tilde{\gamma}_s)\Omega^*(t)C(t) + \sqrt{2\gamma_s/\tilde{\gamma}_s^2} S_{\text{in}}(t) \quad (4)$$

$$\partial_t C(t) = [-f_s |\Omega(t)|^2 - \tilde{\gamma}_c] C(t) + i g_s \Omega(t) S_{\text{in}}(t). \quad (5)$$

where $f_s = \alpha^2/\tilde{\gamma}_s$, $g_s = \alpha\sqrt{2\gamma_s/\tilde{\gamma}_s^2}$.

The second crucial assumption is that the cavity has very high finesse (is a very “good” cavity) for the C -band ($\tilde{\gamma}_c \approx 0$), and the entire process takes place well before any amplitude from $C(t)$ has leaked out. Dropping the $\tilde{\gamma}_c C(t)$ term, the solution to eq. 5 is

$$C(t) = i g_s e^{-f_s \epsilon(t)} \int_{-\infty}^t e^{f_s \epsilon(t')} \Omega(t') S_{\text{in}}(t') dt', \quad (6)$$

where $\epsilon(t) = \int_{-\infty}^t |\Omega(t'')|^2 dt''$. The SFG-cavity mode amplitude at the end of the process $C(\infty)$ equals zero for any $S_{\text{in}}(t')$ that is orthogonal to $e^{f_s \epsilon(t')} \Omega^*(t')$. The function $e^{f_s \epsilon(t')} \Omega^*(t')$ is thus

the optimal TM for storage in this cavity. Hence, the process is perfectly temporal-mode selective, within the approximations made here. The perfect discrimination arises from the fact that the Green's function appearing in the integral for $C(\infty)$ is $e^{-f_s \epsilon(t)} e^{f_s \epsilon(t')}$, which is separable in the input and output variables t, t' . Define the optimal input TM as:

$$S_{in,opt}(t) = N \Omega^*(t) \exp \left[f_s \int_{-\infty}^t |\Omega(t')|^2 dt' \right], \quad (7)$$

where $N = \sqrt{2f_s/(e^{2f_s} - 1)}$ ensures that the square of $S_{in,opt}(t)$ integrates to 1.

This dichroic-finesse cavity scheme is not only highly TM discriminatory, but is also highly efficient, under the assumption that there are negligible internal dissipative losses, that is $\tilde{\gamma}_s = \gamma_s$. In this case, the efficiency is unity if the output field $S_{out}(t)$ is zero. In the case that the input is given by eq. 6, the total unconverted signal energy (photon number) behaves as $W_{out} \rightarrow \exp(-2f_s)$, the trend toward zero being achieved with increasing f_s . This prediction is valid only up to a certain value of control field strength, beyond which the system is driven out of the bad-cavity regime and the conversion efficiency degrades, as we discuss below.

To verify the scheme operates as a high-selectivity quantum pulse gate, we solve the more accurate eqs. 1 and 2 numerically. Unless stated otherwise, the control field is taken to be Gaussian, $\Omega(t) = (2/\pi)^{1/4} \exp[-(t-3)^2]$. Time units are relative to the duration of this dimensionless control pulse. The first goal is to show that the optimal input pulse, designed according to eq. 7, leads to efficient transfer of incoming energy into the frequency-converted cavity mode. (We continue to assume negligible internal cavity loss.)

Figure 2 shows simulation results in the dichroic-finesse cavity scenario, for the case $\gamma_s = 10.1$ and $\gamma_c = 0.010$, or dimensionless cavity lifetimes $1/\gamma_s = 0.09$, $1/\gamma_c = 99.99$. The value of nonlinear coupling, dependent on control pulse energy, is optimized to be $\alpha = 5.5$. As expected, larger values begin to drive the system out of the bad-cavity regime and worsen the conversion efficiency (not shown). The integrated signal input energy equals 1.

Figures 2a and 2b show the result for the case that the input (“red”) signal shape $S_{in,Gaussian}$ is identical in shape to the control pulse Ω , not the optimal case. The “red” cavity mode S reaches a maximum of about 0.2 before rapidly decaying. The converted “blue” cavity mode amplitude, plotted as $-iC$, reaches a value 0.8 before it begins a slow exponential decay into the output channel C_{out} . The “red” output channel S_{out} shows significant leakage and thus poor storage efficiency. The unconverted signal energy W_{out} equals 0.36 in this case with a non-optimized input pulse shape.

Figures 2c and 2d show the case that the input signal shape is given by eq. 6, which is predicted to be optimal. In this case the unconverted signal energy W_{out} equals 0.016, meaning less than 2% of the incoming pulse is not initially trapped in the frequency-converted cavity mode. Correspondingly, the trapped “blue” mode amplitude reaches a value near 1.0 before it begins a slow exponential decay. This means that a properly designed input pulse can achieve high storage efficiency, analogously to results found in atomic-based quantum memories [23].

Any TM orthogonal to the optimal mode given, by eq. 7, is predicted to pass through the cavity system and not frequency convert. Figure 3 shows numerical solutions of eqs. 1 and 2 for two such modes, and, indeed the conversion efficiency is very small for each. Orthogonal modes, denoted mode 1, mode 2, and so on, are constructed numerically using a Gram-Schmidt procedure starting from the optimal mode used earlier in Fig. 2.

Figure 3a shows as the dashed curve the “red” input mode 1, which resembles a Hermite-Gaussian-1 function. The converted “blue” cavity mode amplitude $-iC$ reaches a value -0.7 then rapidly returns to a small value around -0.1 before beginning a slow exponential decay into the output channel C_{out} . The unconverted “red” output channel S_{out} in Fig. 3b shows large leakage. The unconverted signal energy W_{out} equals 0.98 in this case, that is it remains nearly completely

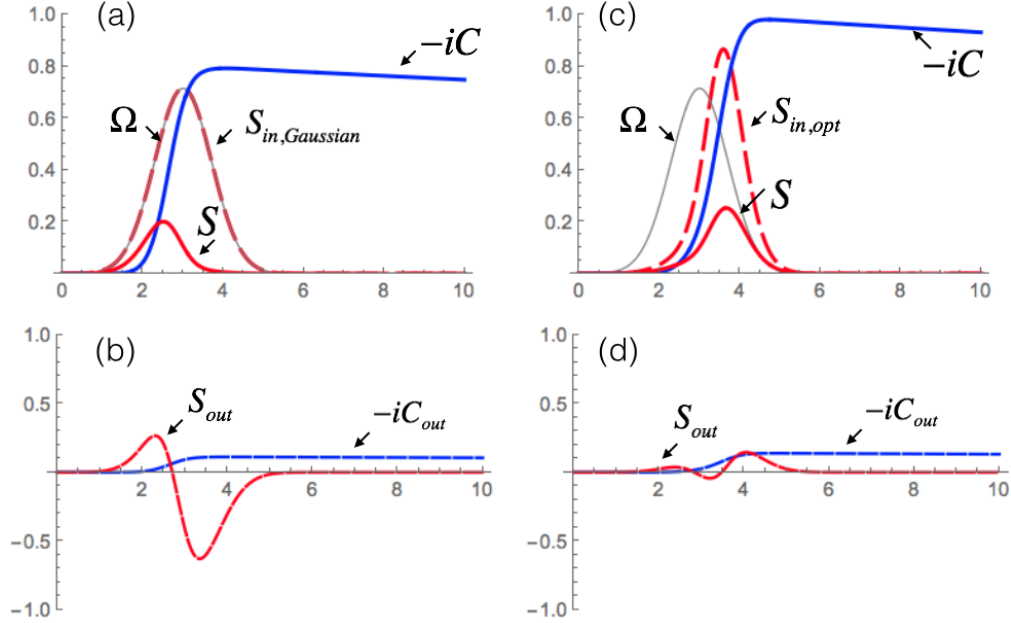


Fig. 2. Numerical simulations of amplitude versus time for (a, b) Gaussian signal input and (c, d) the optimal input temporal mode. The input signal S_{in} and the control pulse Ω are multiplied by 0.8 for convenient plotting. Parameters for both cases: $\alpha = 5.5$, $\gamma_s = 10.1$, $\gamma_c = 0.01$.

unconverted. Figure 3c shows as the dashed curve the “red” input mode 2, which resembles a Hermite-Gaussian-2 function. The converted “blue” cavity mode amplitude $-iC$ oscillates and rapidly returns to a near-zero value, and the “red” output channel S_{out} in Fig. 3d shows large leakage. The unconverted signal energy W_{out} equals 0.99 in this case, again consistent with expectations.

The simulations support our proposal for an all-optical cavity-based demultiplexer: we have shown that given a Gaussian control pulse, there is one optimal signal TM that can be frequency converted efficiently and stored for a time in the cavity, while any mode that is temporally orthogonal to the optimal mode is not frequency converted and passes through the system. The contrast between energy conversion and nonconversion is about 50:1 for the parameters and pulses used, far better than any single-stage QPG based on traveling-wave SFG.

From a different perspective, if we choose any particular targeted “red” signal input TM that we wish to convert to “blue” and store in the dichroic-finesse cavity, we can design the control field that optimizes its conversion and trapping, while not converting any orthogonal signal TM. The condition that ensures near-100% conversion of the “red” input pulse is $S_{out}(t) = 0$, which from eq. 3 implies $S_{in}(t) = \sqrt{2\gamma_s}S(t)$. Then using the bad-cavity approximation for S , as given by eq. 4, leads straightforwardly to $\partial_t C(t) = K(t)C(t)$ and $S_{in}(t) = \mu^* \sqrt{2K}C(t)$, where $K(t) = \int_s |\Omega(t)|^2$ and $\mu = i \exp\{i \arg[\Omega(t)]\}$. From these, one can derive the design equation for $K(t)$:

$$\left(\frac{\partial_t K}{2K}\right) + K(t) = \frac{\partial_t S_{in}(t)}{S_{in}(t)}. \quad (8)$$

An equation of this form also appears in the context of optical storage in cavity-enhanced atomic quantum memories, where it is called the “impedance matching condition.” [21]. The resulting solution for the control field for optimal storage is (See the Appendix.)

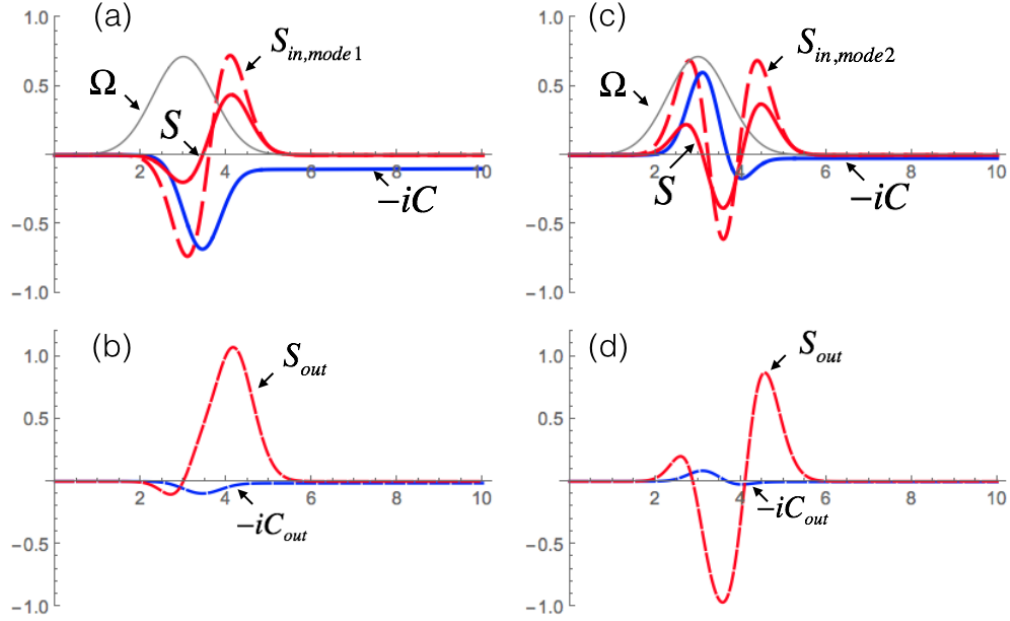


Fig. 3. Numerical simulations of amplitude versus time for two temporal modes that are orthogonal to the optimum TM used in Fig. 2. Both remain nearly completely unconverted. Same parameters and plotting as in Fig. 2.

$$\Omega_{opt}(t) = e^{i\theta} e^{-i \arg[S_{in}(t)]} \sqrt{\frac{S_{in}(t)^2}{q + 2f_s \int_{t_0}^t S_{in}(t')^2 dt'}}, \quad (9)$$

where θ is an arbitrary phase and $q = S_{in}(t_0)^2/|\Omega(t_0)|^2$, which for numerical purposes is a vanishingly small parameter if the arbitrary initial time t_0 is taken to be well before the input signal begins rising from zero value.

To illustrate and test this design prediction, consider as a target input signal any of the orthogonal Hermite Gaussians, $HG_n(t) = H_n(t)e^{-t^2/2}/\sqrt{2^n \pi^{1/2} n!}$. We numerically solve eqs. 1 and 2 using eq. 9 as the control field, and plot the results in fig. 4, where Figs. 4a and 4b show the results for $S_{in}(t) = HG_0(t)$ and $HG_1(t)$, respectively. The value of the control strength parameter α is again optimized to the value 5.5. The shapes of the control fields before the signal begins turning on are arbitrary, and set by the value 10^{-7} of the parameter q . The unconverted signal energy in case (a) is 0.004, and in case (b) is 0.015, showing excellent conversion and trapping of the targeted input TMs.

If we choose the unit time scale in the simulations as 100 ps, the duration of the control pulse in Fig. 2 is 166 ps. Assuming a round-trip time 15 ps and group velocity $c/2$ gives a cavity round-trip length $225 \mu\text{m}$. The cavity leakage parameters ($\gamma_s = 10.1$, $\gamma_c = 0.01$) corresponding to rates $1.01 \times 10^{11} \text{s}^{-1}$ and $1.0 \times 10^8 \text{s}^{-1}$ (and cavity-field lifetimes 10 ps and 10 ns) respectively. For carrier wavelengths 1550 nm and 775 nm for S and C modes, respectively, the ‘‘dichroic’’ cavity quality factors needed are $Q_s = \omega_s/2\gamma_s = 6020$ and $Q_c = \omega_c/2\gamma_c = 1.2 \times 10^7$. Finally, the internal dissipative losses need to be much smaller than γ_s , γ_c . These values, along with the needed control power, are within range of achievable values for whispering-gallery resonators or planar-waveguide micro-rings coupled evanescently to an external waveguide.

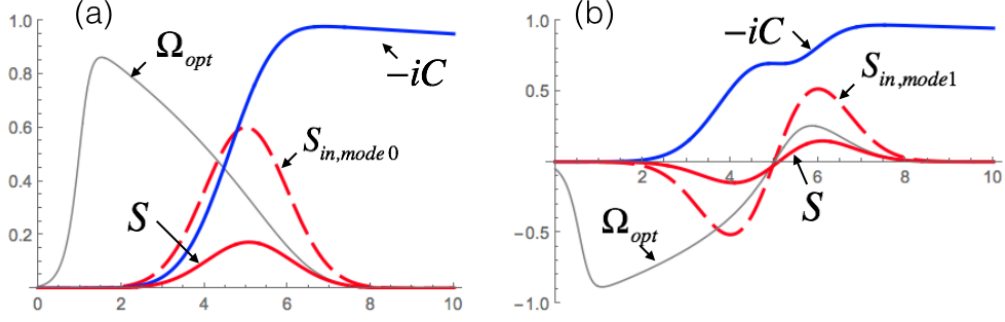


Fig. 4. Illustrating the effectiveness of the control field $\Omega_{opt}(t)$ to efficiently convert and store the targeted “red” input mode $S_{in}(t)$. (a) $S_{in}(t) = HG_0(t)$, (b) $S_{in}(t) = HG_1(t)$. In both cases, using the designed control field drives the converted cavity mode amplitude $-iC$ to near its maximum possible value of 1.0. In both cases: $\alpha = 5.5$, $\gamma_s = 10.1$, $\gamma_c = 0.01$, $q = 10^{-7}$.

In summary, the newly proposed scheme offers several functionalities crucial for quantum information science. It can multiplex and demultiplex orthogonal temporal modes of light with high TM discrimination and efficiency. It is reconfigurable in real time to target any chosen TM by altering the shape of the control field that drives the sum-frequency generation. The efficiency of TM demultiplexing is tunable in real time by altering the intensity of the control field, giving the possibility to create and measure single-photon states that are superpositions of two time-bin states. It can be used as a short-time all-optical memory, the storage time being limited by cavity Q and losses. And it can be used to reshape optical pulses via the read-in, read-out process.

The vast majority of time-stationary optical processes satisfy the Fourier constraint, $\Delta\omega_P\Delta t_P \approx 2\pi$, where $\Delta\omega_P$ and Δt_P are the bandwidth and processing (interaction, or read-out) time of the process. (Rare exceptions may occur in systems lacking Lorentz (time-reversal) reciprocity [34].) Our system, being time-nonstationary, has the useful property that both the bandwidth and the storage time, while not being bound by $\Delta\omega_P\Delta t_P \approx 2\pi$, are tunable in real time. The read-in bandwidth $\Delta\omega_P$ for the input channel is set by the shape of the control field $\Omega(t)$, while the read-out time Δt_P in the output channel is set either by the natural decay time of the narrow C mode resonance (which is much narrower than that of the input S mode resonance) or by the duration of the outgoing red signal pulse in cases where a read control pulse is employed.

Acknowledgements: We thank Hailin Wang for helpful discussions. DVR and MGR were supported by NSF grant no. 1521466.

Appendix

The solution of eq. 8 for the optimum coupling function is

$$K(t) = \frac{K(t_0)S_{in}(t)^2}{S_{in}(t_0)^2 + 2K(t_0) \int_{t_0}^t S_{in}(t')^2 dt'} \quad (10)$$

Using $K(t) = f_s|\Omega(t)|^2$ and $\mu = i \exp\{i \arg[\Omega(t)]\}$ gives

$$\mu\sqrt{2K(t)} = i e^{i \arg[\Omega(t)]} \sqrt{2f_s} \sqrt{|\Omega(t)|^2} = i\sqrt{2f_s}\Omega(t) \quad (11)$$

Therefore

$$\mu\sqrt{2K(t)} = i e^{i \arg[\Omega(t)]} \sqrt{2f_s} \sqrt{|\Omega(t)|^2} = i\sqrt{2f_s}\Omega(t) \quad (12)$$

$$\Omega_{opt}(t) = \frac{\mu\sqrt{2K(t)}}{i\sqrt{2f_s}} = e^{i \arg[\Omega(t)]} \sqrt{\frac{K(t)}{f_s}} = e^{i \arg[\Omega(t)]} \sqrt{\frac{S_{in}(t)^2}{S_{in}(t_0)^2 f_s / K(t_0) + 2f_s \int_{t_0}^t S_{in}(t')^2 dt'}} \quad (13)$$

$$\Omega_{opt}(t) = e^{i \arg[\Omega(t)]} \sqrt{\frac{S_{in}(t)^2}{S_{in}(t_0)^2 / |\Omega(t_0)|^2 + 2f_s \int_{t_0}^t S_{in}(t')^2 dt'}} \quad (14)$$

For the optimum input TM case, the time-derivative of $C(t)$ in eq. 5 should always have the same phase, as we require that $|C(t)|$ grow monotonically. For the second term in the right-hand side of eq. 5 to have constant phase for arbitrary input $S_{in}(t)$, we need $\arg[\Omega_{opt}(t)] = \theta - \arg[S_{in}(t)]$, leading posthaste to eq. 9.

$$\mu\sqrt{2K(t)} = i\sqrt{2f_s} e^{i \arg[\Omega(t)]} \sqrt{|\Omega(t)|^2} = i\sqrt{2f_s}\Omega(t) \quad (15)$$

$$\Omega_{opt}(t) = e^{i\theta} e^{-i \arg[S_{in}(t)]} \sqrt{\frac{S_{in}(t)^2}{q + 2f_s \int_{t_0}^t S_{in}(t')^2 dt'}} \quad (16)$$